J Mater Sci (2011) 46:4236–4242
DOI 10.1007/s10853-011-5247-8

Martensitic interfaces and transformation crystallography in Pu–Ga alloys

Xiao Ma · Robert C. Pond

Received: 27 August 2010 / Accepted: 6 January 2011 / Published online: 20 January 2011

Abstract The face-centered cubic (δ) to monoclinic (α) martensitic transformation in Pu–Ga is unusual because it produces a relative large change of volume up to 20%. Moreover, the transformation crystallography is not predicted satisfactorily by the classical phenomenological theories of martensite crystallography, which is based on the hypothesis that the habit plane is an invariant plane of the total shape change. In this study we use the recently developed topological model where the habit plane, i.e., the interface between the parent and martensite phases, is envisaged as a semi-coherent configuration with coherent terraces reticulated by a network of disconnections or transformation dislocations, and defects producing lattice-invariant deformation. The authors show explicitly that this network not only accommodates the coherency strains, so that no long-range strain field arises, but also produces diffusionless transformation by motion of the disconnections across the interface. It was show that the predicted habit plane inclination with respect to the parent and martensite phases in a Pu–Ga alloy is in good agreement with published experimental observations when the lattice-invariant deformation is $(201)_\alpha/[10\bar{2}]_\alpha$ twinning, as observed experimentally.

X. Ma (✉)
School of Materials Science and Engineering, South China University of Technology, 510640 Guangzhou, People's Republic of China
e-mail: maxiao@scut.edu.cn

R. C. Pond
School of Engineering, Computing and Mathematics, University of Exeter, North Park Road, Exeter EX4 4QF, United Kingdom

Introduction

Plutonium is an important nuclear material due to its highly radioactive properties. Stabilized plutonium compounds, such as Pu–Ga alloys, undergo a diffusionless transformation, generally considered via martensitic mechanism [1], when cooling from the face-centered cubic (FCC) δ phase to the monoclinic α phase. The martensitic transformation of Pu–Ga alloys is of interest in terms of transformation crystallography analysis because it is associated with an unusually large 20% volume contraction [2], and one would like to explore whether the crystallographic requirements for a martensitic mechanism are met and predictable in such system. There have been a number of studies of the transformation crystallography in Pu–Ga alloys [3, 4], as reviewed by Hecker et al. [1]. However, the crystallography analysis presented in most of the existing publications were followed the classical phenomenological theory of martensite crystallography (PTMC) procedure developed by Wechsler et al. [5] and Bowles and Mackenzie [6] in the 1950s, based on the notion that the interface between the parent and product phases is an invariant plane of the shape deformation. Recently, an alternative model of martensitic transformations based on dislocation theories has been put forward by Pond and Hirth [7, 8], refer to as the topological model (TM). This approach first considers the atomic structure of the interface between the parent and product phases and determines the viable interfacial defects arise therein, and then predicts a consistent habit plane and lattice orientation relationship directly from the geometry of the defects. In the following sections, the principles of the TM are outlined and subsequently applied to Pu–Ga alloys. Finally, experimental observations of transformations in Pu–Ga systems previously reported in the literature are compared with the present modelling results.

Topological model of martensitic interfaces

The structure of the parent–martensite interface is a key issue governing martensitic transformations. According to the TM, the structure of martensitic interfaces comprises coherent terraces with an array of interfacial dislocations superimposed. The terrace configuration is supposed to have relatively low interfacial energy, and to require the abutting crystals to be strained into coherency in general. These coherency strains are accommodated by the interfacial dislocation array. For most cases, at least two sets of non-parallel defects will be needed in order that no long-range stress remains. One of these sets comprises lattice invariant deformation (LID) defects, i.e., slip or twinning dislocations of the product phase, and the other comprises transformation dislocations or disconnections. Lateral motion of the disconnections will cause the product phase to grow, and this will be diffusionless in the truly martensitic case. A detailed description of the TM could be found elsewhere [9, 10], and the basic procedure of modelling a martensitic transformation using the TM is summarized as follows,

1. A coherent terrace is identified; the two crystals, initially exhibiting their natural lattice parameters and disposed in a chosen orientation relationship (OR) known as the *natural reference state*, are strained into coherency on the selected terrace plane (TP), thereby forming the *coherent reference state*. The selection of a feasible reference state is highly constrained if the transformation process is to be diffusionless.
2. The topological character, (**b**, 0) and (**b**, h), of dislocations and glissile disconnections, respectively, are identified in the coherent reference state, and the glissile nature of their intersections confirmed.
3. The array of interfacial defects necessary to accommodate the coherency strain is determined in terms of their line directions, ξ^{D} and ξ^{L}, and spacings, d^{D} and d^{L}, where the superscripts D and L refer to disconnections and LID, respectively. This enables the habit plane to be determined, and the OR between the natural crystals is found from the rigid-body rotation introduced by the defect array.

The δ to α transformation in Pu–Ga alloys

Coherency strains

An important crystallographic feature of the martensitic transformation in Pu–Ga is the near parallelism of the $(111)_{\delta}$ and $(010)_{\alpha}$ planes, and the $[\bar{1}10]_{\delta}$ and $[100]_{\alpha}$ directions [11]. These two planes are candidate terrace planes according to the topological arguments demonstrated in [9]. Schematic scale drawings of the terraces in the δ and α phases are depicted in Fig. 1a, b, respectively; the two crystals are exhibiting their natural lattice parameters [12] as listed in Table 1. Crocker [13] introduced a HCP pseudostructure to replace the conventional monoclinic description of the martensite phase in Pu–Ga alloys. As indicated in Fig. 1c, the $(0\bar{1}0)_{\alpha}$ plane is related to the $(000\bar{1})$ basal plane in a HCP lattice, and the $[100]_{\alpha}$, $[\bar{1}02]_{\alpha}$, and $[\bar{3}02]_{\alpha}$ directions correspond to the $<11\bar{2}0>_{HCP}$ directions. This pseudostructure has distorted hexagonal unit cells in the terrace plane and the stacking order of these planes is ABABAB. While in the parent phase, the

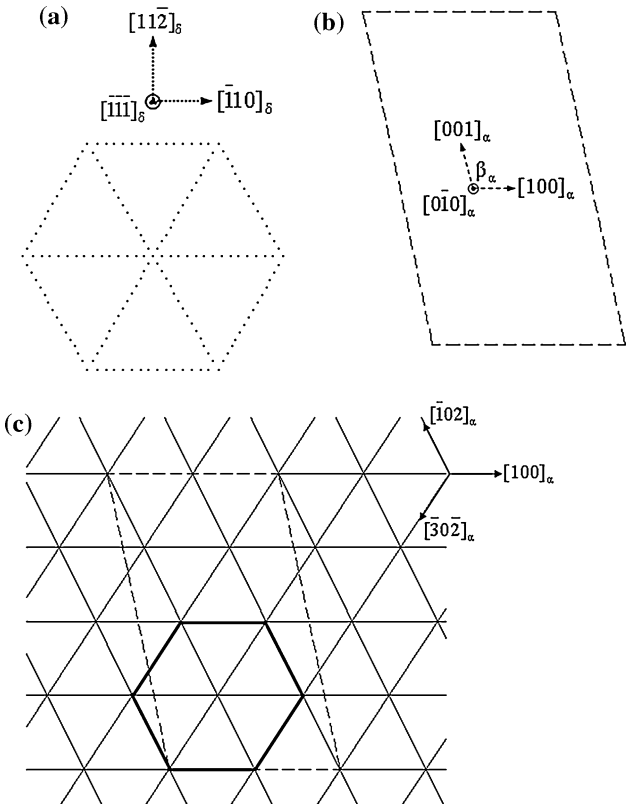

Fig. 1 Schematic illustration of the **a** $(111)_{\delta}$ and **b** $(010)_{\alpha}$ terrace plane in Pu–Ga. **c** HCP pseudostructure (*solid lines*) description of the conventional monoclinic lattice (*dashed lines*) of the martensite phase. The distorted hexagon unit cell of the pseudo-HCP lattice is highlighted by *bold lines*

Table 1 Lattice parameters of the FCC (δ) and monoclinic (α) phases of a Pu–Ga alloy exhibiting their natural reference states (after Lawson et al. [12])

a_{δ}(nm)	a_{α}(nm)	b_{α}(nm)	c_{α}(nm)	β_{α}(°)
0.4626	0.6199	0.4630	1.0700	101.82

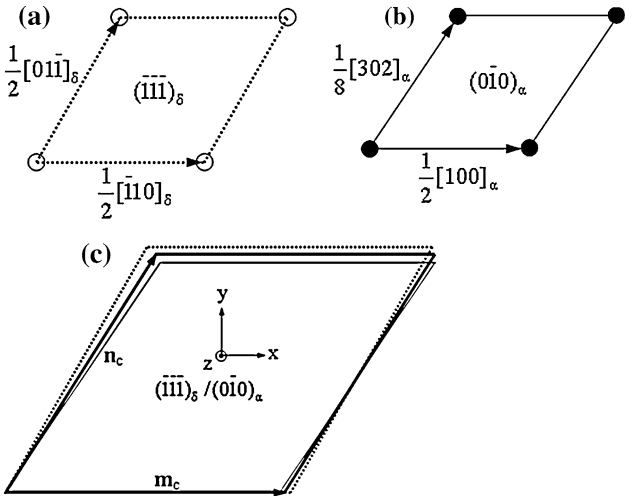

Fig. 2 Schematic drawing showing the corresponding vectors in **a** the $(\overline{111})_\delta$ terrace plane and **b** the $(0\bar{1}0)_\alpha$ terrace plane. **c** The coherent reference state (*bold lines*) is formed as an intermediate configuration between the two natural lattices

$(111)_\delta$ terrace planes consist of perfect hexagons and the stacking sequence is ABCABC. To determine the coherent reference terrace relating the two natural ones, it is convenient to consider the corresponding unit parallelogram cells of the parent and martensite terraces as depicted in Fig. 2a, b, respectively. The edges of these cells are translation vectors in the FCC and pseudo-HCP lattices as indicated in the figure. The coherent reference state is an intermediate state of the two natural lattices. Two basic translation vectors, $\mathbf{m}_c$ and $\mathbf{n}_c$, of the coherent unit cell are related to the corresponding natural vectors as depicted in Table 2. Using terrace plane coordinate frame, *xyz*, where *x* is parallel to $[\bar{1}10]_\delta/[100]_\alpha$ and *z* parallel to $[\overline{111}]_\delta/[0\bar{1}0]_\alpha$ as depicted in Fig. 2c, the indices of these vectors, written as 2×1 column vectors, are readily obtained and listed in Table 2. Hence the total coherency strain on the terrace plane, ${}_nE_c$, is given by

$$ {}_nE_c = \left({}_cP_\delta^{-1} - {}_cM_\alpha^{-1}\right), \qquad (1) $$

where ${}_cP_\delta$ and ${}_cM_\alpha$ are 2×2 matrices representing the deformations from δ and α to the coherent reference state on the terrace plane, respectively.

Interfacial defects

Candidate disconnections are conveniently identified in the coherent dichromatic pattern of the terrace plane and three examples are depicted in Fig. 3a, their Burgers vectors corresponding to black-to-white vectors, $t_c(\delta) - t_c(\alpha)$. One is designated $b^D_{p/q}$ to indicate that the disconnection's step goes upwards (p, q > 0) into the parent crystal by |p| terrace planes of δand |q| terrace planes of α; in contrast, the step goes downwards into the martensite crystal if p, q < 0. For glissile disconnections, *p* must equal to *q*. Figure 3b further illustrates the step height of one of the admissible disconnections, $b^D_{+2/+2}$, when viewing along $[01\bar{1}]_{\delta'}$. The corresponding translation vectors are $t_c(\delta) = \frac{1}{2}[\overline{211}]_{\delta'}$ and $t_c(\alpha) = [0\bar{1}0]_{\alpha'}$. The z component of this disconnection, b^D_z, is equal to the difference of the surface step heights, $h(\delta) - h(\alpha)$, where $h(\delta) = 2d_{(111)\delta'}$ and $h(\alpha) = d_{(010)\alpha'}$. Please be aware that δ' and α' are used to indicate the coherently strained FCC and monoclinic phases, respectively, and to distinguish from the natural unstrained parent and martensite phases, δ and α.

For the LID consideration, twins are commonly observed in Pu–Ga using optical microscopy, but the exact twinning system is uncertain for a long period due to insufficient quantitative experiments. Crocker [13] studied the crystallography of deformation twinning in α-Pu theoretically and tabulated twenty possible twinning modes with relatively small shear magnitudes. Zocco et al. [14] reported that two candidate modes, $(201)_\alpha/[10\bar{2}]_\alpha$ and $(205)_\alpha/[\bar{5}02]_\alpha$ [15], have been observed recently, and these modes are consistent with Crocker's suggestion. In this study, it was considered that the twinning plane to be $(201)_\alpha$ and the Burgers vector, b^L, of the twinning dislocation is $\frac{1}{32}[10\bar{2}]_\alpha$ as illustrated in Fig. 4. The magnitude of the twinning Burgers vector, $|b^L|$, is equal to 0.0775 nm, which is consistent with Crocker's analysis [13].

Interface structure

The coherency strains arise at the terrace plane as given by expression (1) must be relieved by arrays of interfacial defects in the habit plane. As demonstrated in Pond et al.

Table 2 Indices of the basic translation vectors in the natural and coherent reference lattices expressed in the terrace plane *xyz* coordinate frame

m_δ	n_δ	m_α	n_α	m_c	n_c
$\frac{1}{2}[\bar{1}10]_\delta$	$\frac{1}{2}[01\bar{1}]_\delta$	$\frac{1}{2}[100]_\alpha$	$\frac{1}{8}[302]_\alpha$	$\frac{1}{2}(m_\delta + m_\alpha)$	$\frac{1}{2}(n_\delta + n_\alpha)$
$\begin{pmatrix} 0.3271 \\ 0 \end{pmatrix}$	$\begin{pmatrix} 0.1636 \\ 0.2833 \end{pmatrix}$	$\begin{pmatrix} 0.3099 \\ 0 \end{pmatrix}$	$\begin{pmatrix} 0.1777 \\ 0.2618 \end{pmatrix}$	$\begin{pmatrix} 0.3185 \\ 0 \end{pmatrix}$	$\begin{pmatrix} 0.1706 \\ 0.2726 \end{pmatrix}$

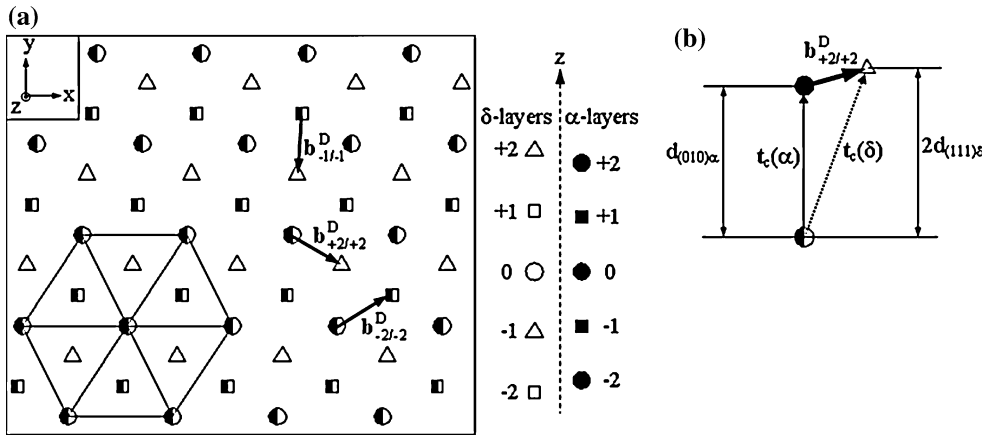

Fig. 3 **a** Dichromatic pattern of the coherent $(\overline{1}11)_{\delta'}/(0\overline{1}0)_{\alpha'}$ terrace plane, white symbols represent the δ lattice sites and *black symbols* the α, their stacking sequence along z is associated with the designated shapes showing on the right. The Burgers vectors of three candidate disconnections are indicated by *bold arrows*. **b** The step character of the disconnection $b^{D}_{+2/+2}$ is shown when viewed along its line direction, which is taken to be $[01\overline{1}]_{\delta'}$ for illustrative purposes

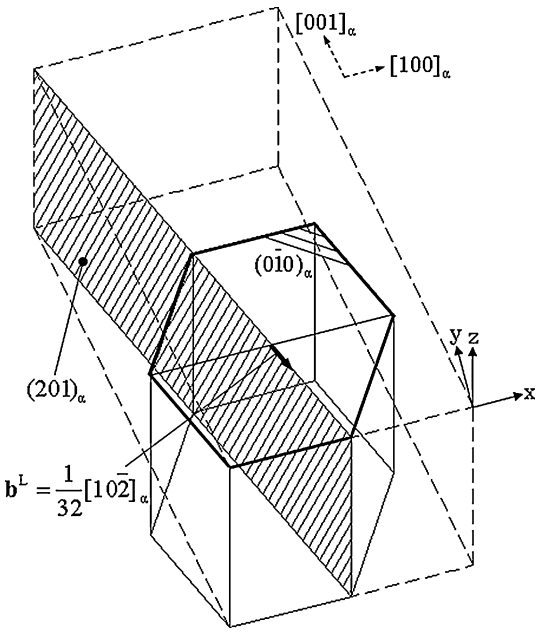

Fig. 4 Schematic illustration showing the $(201)_\alpha/[10\bar{2}]_\alpha$ twinning system in Pu–Ga. The twinning plane is depicted by hatched area and the twinning shear direction is indicated by the *bold arrow*. A monoclinic cell is depicted by *dashed lines* and a pseudo-HCP cell is outlined by *solid lines*, the terrace plane is indicated by *bold lines*

[9], provisional defect arrays in the terrace plane are determined firstly by suppressing the z component of the interfacial defects. According to the TM arguments, the line direction of disconnections, ξ^{D}, and the LID line direction, ξ^{L}, could be determined once the Burgers vectors of the defects and the total coherency strain arising on the terrace plane are defined, as shown in previous sections. One has

$$\xi^{D} = \frac{\pm({}_{n}E_{c})^{-1}\cdot b^{L}}{\left|({}_{n}E_{c})^{-1}\cdot b^{L}\right|}, \tag{2a}$$

and

$$\xi^{L} = \frac{\pm({}_{n}E_{c})^{-1}\cdot b^{D}_{+2/+2}}{\left|({}_{n}E_{c})^{-1}\cdot b^{D}_{+2/+2}\right|}. \tag{2b}$$

Hence the angle from the positive x axis to these line directions, θ^{D} and θ^{L}, are readily obtained. Therefore, the spacings of the disconnection and the LID arrays, d^{D} and d^{L}, can be determined by

$$d^{D} = \frac{\left|b^{D}_{+2/+2}\right|}{\left|{}_{n}E_{c}\cdot\xi^{L}\right|}\sin\left|\left(\theta^{D}-\theta^{L}\right)\right| \tag{3a}$$

and

$$d^{L} = \frac{|b^{L}|}{\left|{}_{n}E_{c}\cdot\xi^{D}\right|}\sin\left|\left(\theta^{D}-\theta^{L}\right)\right| \tag{3b}$$

A schematic illustration of the provisional defect network on the terrace plane so obtained is depicted in Fig. 5.

As illustrated in Fig. 3b, the step height, h, of disconnection $b^{D}_{+2/+2}$ is equal to the smaller terrace interplanar spacing, $d_{(010)\alpha'}$. The first refined habit plane, HP^{1}, is deviated from the terrace plane by the angle ψ^{1} about ξ^{D} due to the step character of disconnections, and one has $\psi^{1} = \tan^{-1}\left(\frac{h(\alpha)}{d^{D}}\right)$. To seek for the defect network that relieves the coherency strains on the HP^{1}, one has to re-express the coherency strains and the Burgers vectors of the disconnection and LID using the HP^{1} (primed) coordinate frame, where x' parallel to ξ^{D}, and, y' rotates about

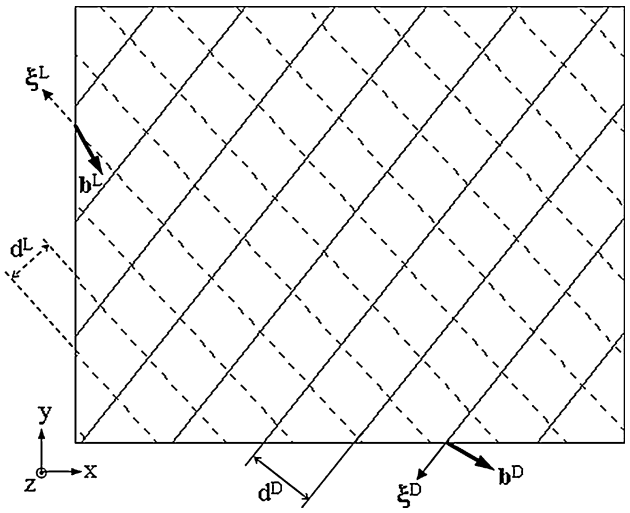

Fig. 5 Schematic illustration of a provisional misfit-relieving defect network on the terrace plane in Pu–Ga. *Solid* and *dashed lines* represent the disconnection and LID arrays, respectively, their Burgers vectors and spacing also shown

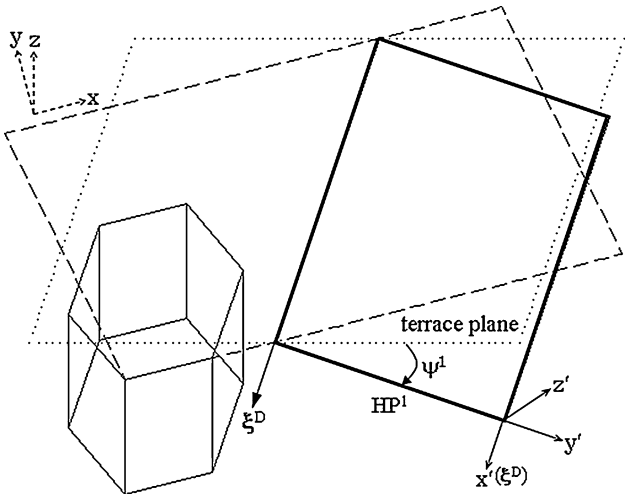

Fig. 6 Schematic illustration of the HP^1 (*bolded lines*) which is obtained by, firstly, rotating the terrace plane (*dashed lines*) about z by θ^D so *x*-axis parallel to ξ^D, and then the rotated terrace plane (*dotted lines*) is further rotated by the angle ψ^1 about ξ^D

ξ^D from the TP by the angle ψ^1 as depicted in Fig. 6. The coordinate transformation from the TP frame to the HP^1 frame is represented by the matrix ${}_{HP^1}T_{TP}$ and

$$ {}_{HP^1}T_{TP} = \begin{pmatrix} 1 & 0 & 0 \\ 0 & \cos(\psi^1) & -\sin(\psi^1) \\ 0 & \sin(\psi^1) & \cos(\psi^1) \end{pmatrix} \begin{pmatrix} \cos(\theta^D) & \sin(\theta^D) & 0 \\ -\sin(\theta^D) & \cos(\theta^D) & 0 \\ 0 & 0 & 1 \end{pmatrix}. \quad (4) $$

When expressed in the HP^1 frame, the coherency strain, ${}_nE'_c$, is given by

$$ {}_nE'_c = {}_{HP^1}T_{TP} \cdot {}_nE_c \cdot {}_{HP^1}T^T_{TP} \quad (5) $$

Similar to the analysis of the misfit-reliving defect array on the TP presented above, one obtains the parameters of the defect network that removes the coherency strains on the HP^1. The spacings of disconnection and LID arrays on the HP^1, $d^{D'}$ and $d^{L'}$, are 1.4671 and 1.1002 nm, respectively. Therefore, the inclination of the habit plane obtained by the second order of refinement, ψ^2, becomes $\sin^{-1}\left(\frac{h(\alpha)}{d^{D'}}\right)$ and determined to be 18.39°.

Transformation crystallography

When a refined habit plane is obtained, the Burgers vector components of disconnections and LID normal to the habit plane are designated as $b_z^{D'}$ and $b_z^{L'}$, respectively. These components do not contribute to the strain accommodation on the habit plane, but constitute tilt walls causing rigid-body rotations, φ^D and φ^L, of the transforming crystals about an axis parallel to ξ^D and ξ^L, respectively, and one has

$$ \varphi^D = 2\sin^{-1}\left(\frac{b_z^{D'}}{2d^{D'}}\right), \quad (6a) $$

and

$$ \varphi^L = 2\sin^{-1}\left(\frac{b_z^{L'}}{2d^{L'}}\right), \quad (6b) $$

where $d^{D'}$ and $d^{L'}$ are the spacings of the disconnection array and LID array on the refined habit plane, respectively. The configuration of a tilt-wall is analogous to the low angle tilt grain boundary. As a result, the initial chosen OR of the parent and product crystals is modified. The tilt due to the disconnections is depicted in Fig. 7b; the two crystals are misorientated by the angle $\varphi^D = 4.65°$ about ξ^D beyond the interfacial distortion field. The determination of the total misorientation deviated from the initially chosen OR needs to consider the contribution from both the φ^D and φ^L, the latter is suppressed in this approximation.

Consider the φ^D being partitioned into the two crystals equally, the habit plane inclinations with respect to the $(\overline{111})_\delta$ and $(0\bar{1}0)_\alpha$ plane in the relaxed crystals beyond the interfacial distortion field are given by

$$ \psi_\delta = \psi^2 - \frac{\varphi^D}{2}, \quad (7a) $$

and

$$ \psi_\alpha = \psi^2 + \frac{\varphi^D}{2}, \quad (7b) $$

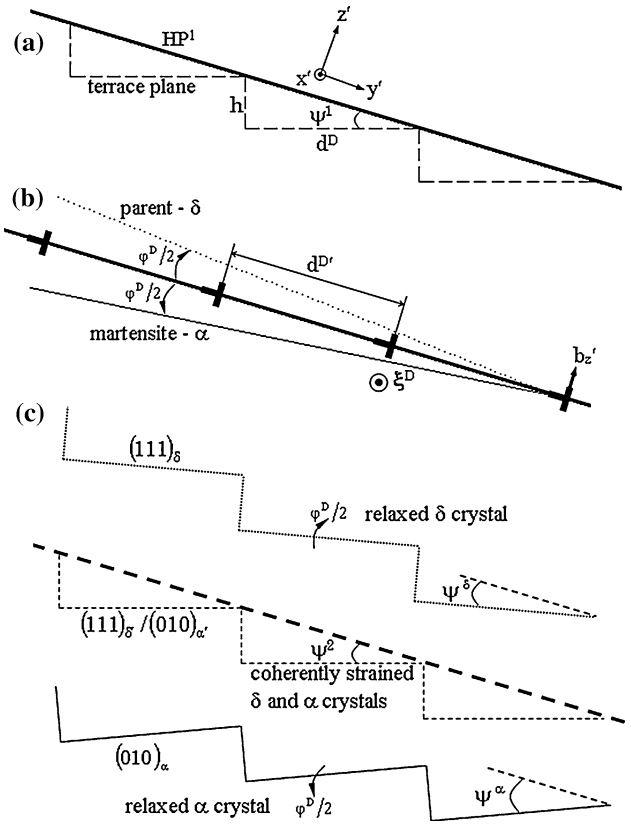

Fig. 7 **a** Schematic illustration of the terrace/step structure of habit plane in Pu–Ga. **b** A tilt-wall is formed due to the $b_z^{D'}$ component of the disconnections, and the tilt is partitioned into the parent and martensite crystals by equal amount. **c** The parent and martensite crystals are rotated by the angle $\varphi^D/2$ with opposite sense about ξ^D,respectively, beyond the interfacial distortion field, and thus the inclinations of the habit plane with respect to the terrace planes in relaxed crystals are established

respectively, as illustrated in Fig. 7, where $\psi_\delta = 16.07°$ and $\psi_\alpha = 20.72°$. The partitioning of the tilt due to the LID array is similar to the arguments presented above. This small correction to the habit plane inclinations is not pursued in this context for simplicity.

Discussion

Due to the reactive and radioactive nature of Pu–Ga alloys, it proved very difficult to perform electron diffraction using conventional TEM. Early studies were mainly concentrated on metallographic examinations and theoretical methods. Recently, Zocco et al. [14, 15] provided direct evidence of twinning within the α phase and measured the habit plane index. Their observations are summarized in Table 3. In contrast to the rare experimental data, a large volume of theoretical investigations have appeared in the

Table 3 Comparison of theoretically predicted and experimentally observed crystallographic information in Pu–Ga alloys

	Experimental observations (Zocco et al. [14, 15])	Theoretical results				
		Present work	Hirth et al. [17]	Adler et al. [4]	Choudhry and Crocker [3]	Zocco et al. [15]
HP_δ	–	–	–	$(.817.538.208)_\delta$	$(.824.5290.199)_\delta$	$(.732.535.422)_\delta$
HP_α	$(1\bar{3}\bar{2})_\alpha$	Close to $(1\bar{3}\bar{2})_\alpha$	–	–	–	$(.148-.908-.391)_\alpha$
$HP_\delta \wedge (\bar{1}\bar{1}\bar{1})_\delta$	–	16.07°	23.1°	25.52°	26.27°	12.818°
$HP_\alpha \wedge (0\bar{1}0)_\alpha$	~ 19.7°	20.72°	16.5°	–	–	11.868°
$(\bar{1}\bar{1}\bar{1})_\delta \wedge (0\bar{1}0)_\alpha$	~ 5°	4.65°	6.6°	2.61°	2.40°	–
LID mode	$(201)_\alpha/[10\bar{2}]_\alpha$ twinning and $(205)_\alpha/[\bar{5}02]_\alpha$ twinning	$(201)_\alpha/[10\bar{2}]_\alpha$ twinning	Twining + slip $(32\bar{3})_\alpha/[101]_\alpha$	$(001)_\alpha/[100]_\alpha$ twinning	$(001)_\alpha/[100]_\alpha$ twinning	$(205)_\alpha/[\bar{5}02]_\alpha$ twinning
ξ^D	$[\bar{2}0\bar{1}]_\alpha$	4.83° from $[\bar{2}0\bar{1}]_\alpha$	$[100]_\alpha$	–	–	9.443° from $[\bar{2}0\bar{1}]_\alpha$

literature. Pertinent works to the present system include those carried out by Adler et al. [4], Crocker [13, 16], Choudry and Crocker [3], and Olsen [11]. However, all of these attempts were based on the PTMC in finding invariant plane strain solutions. Very recently, Hirth et al. [17] presented an alternative solution in terms of the TM and the defect systems proposed by these authors differ from this study. Relevant theoretical results from the studies mentioned above are listed in Table 3 as well.

It is evident from Table 3 that using one of the experimental observed twinning systems, i.e., the $(201)_\alpha/[10\bar{2}]_\alpha$ twins, the habit plane prediction of this study is in better agreement with experiment than that of the PTMC solutions, and a previous TM solution where the LID mode used has not been observed so far. This statement is made not only by comparing the HP inclination angles, because there is an infinity of planes having the same angle with the TP, but also considering the orientation of the intersection of the HP and the TP, which is the line direction of the disconnection as envisaged in Fig. 2 of Pond et al. [9]. Taking into account the sense of the disconnection's step, a set of these two parameters defines a unique HP. The present predicted line direction of disconnections, ξ^D, is 4.8° away from the observed direction; and the discrepancy in terms of the HP inclination angle between the model and the experiment is about 1°.

Another finding from this study is that only the TM can predict a relatively large rigid body rotation, i.e., large angular separation of the $(111)_\delta$ and $(010)_\alpha$ planes, which is consistent to the experimental observations reported previously [11, 15]. The large value of φ^D is expected in the TM because of the large volume change associated with transformations in Pu–Ga and the admissible disconnection has a relative large b_Z^D component. A systematic comparison of the TM and the PTMC by Pond et al. [18] revealed that the value of b_Z^D maybe the key parameter governing the discrepancy between the predictions of the two models. They have shown that the TM and the PTMC yield the same HP when b_Z^D equals to zero in some cases.

Acknowledgements The authors would like to thank Prof. J. P. Hirth for invaluable discussions. XM gratefully acknowledge the financial support from the National Natural Science Foundation of China (Grant no. 50801029) and the Fundamental Research Funds for the Central Universities (SCUT-2009ZM0127, GDNSF-9451064101002833 and SRFDP-200805611031).

References

1. Hecker SS, Harbur DR, Zocco TG (2004) Prog in Mat Sci 49:429
2. Mitchell JN, Stan M, Schwartz DS, Boehlert CJ (2004) Metall Mat Tran 35A:2267
3. Choudry MA, Crocker AG (1985) J Nucl Mater 127:119
4. Adler PH, Olson GB, Margolies DS (1986) Acta Metall 34:2053
5. Wechsler MS, Lieberman DS, Read TA (1953) Trans AIME 197:1503
6. Bowles JS, Mackenzie JK (1954) Acta Metall 2:129
7. Pond RC, Hirth JP (1994) Solid State Phys 47:287
8. Hirth JP, Pond RC (1996) Acta Mater 44:4749
9. Pond RC, Hirth JP, Ma X, Chai YW (2007) In: Nabarro FRN, Hirth JP (eds) Dislocations in solids, vol 13. Elsevier, Amsterdam
10. Pond RC, Ma X, Hirth JP (2008) J Mater Sci 43:3881. doi: 10.1007/s10853-007-2158-9
11. Olsen CE (1989) J Nucl Mater 168:326
12. Lawson AC, Roberts JA, Martinez B, Richardson JW Jr (2002) Philos Mag 82B:1837
13. Crocker AG (1971) J Nucl Mater 41:167
14. Zocco TG, Sheldon RI, Stevens MF, Rizzo HF (1989) J Nucl Mater 165:238
15. Zocco TG, Stevens MF, Adler PH, Sheldon RI, Olson GB (1991) Acta Metall Mater 38:2275
16. Crocker AG (1965) J Nucl Mater 16:306
17. Hirth JP, Mitchell JN, Schwartz DS, Mitchell TE (2006) Acta Mater 54:1917
18. Pond RC, Celotto S, Hirth JP (2003) Acta Mater 51:5385